OPEN ACCESS
IOP Publishing
Journal of Physics D: Applied Physics
J. Phys. D: Appl. Phys. **58** (2025) 475107 (7pp)
https://doi.org/10.1088/1361-6463/ae1e0e

Investigation of defects in 3C-SiC using deep level transient spectroscopy

P U Feiler[1,2,*], T Mchedlidze[2], K Cherkaoui[3], P Ward[3], A Blake[3], J Heitmann[1,2] and F C Beyer[1]

[1] Department of Energy Materials and Test Devices, Fraunhofer Institute for Integrated Systems and Device Technology, Am Sankt Niclas Schacht 13, 09599 Freiberg, Germany
[2] Institute of Applied Physics, TU Bergakademie Freiberg, Leipziger Straße 23, 09599 Freiberg, Germany
[3] Tyndall National Institute, University College Cork, Lee Maltings, Dyke Parade, Cork, T12R5CP, Ireland

E-mail: paul.ulrich.feiler@iisb.fraunhofer.de, Teimuraz.Mtchedlidze@physik.tu-freiberg.de, Johannes.Heitmann@physik.tu-freiberg.de and franziska.beyer@iisb.fraunhofer.de

Received 21 August 2025, revised 4 November 2025
Accepted for publication 11 November 2025
Published 24 November 2025

Abstract

In this work, epilayers of *n*-3C-SiC on Si were investigated using deep level transient spectroscopy (DLTS). The layer structure allowed the investigation of electrically active defects in the *n* type region of 3C-SiC. By comparison with theoretical calculations based on density functional theory supercells in combination with local moment counter charge from the literature, the observed DLTS peaks could be assigned to intrinsic defects, more specifically different clusters of vacancies and silicon interstitials. The defects may be formed due to the different lattice constants of 3C-SiC and Si, similarly to the dislocations and voids previously observed in TEM studies. Our studies suggest that the DLTS peak observed close to 260 K originates from overlapping two intrinsic defects containing a single positively charged carbon vacancy and a single positively charged silicon interstitial.

Keywords: silicon carbide, 3C-SiC, DLTS, deep level transient spectroscopy, electrically active defects

1. Introduction

Silicon carbide (SiC) is an IV–IV-semiconductor with over 170 polytypes [1]. These are composed of different layers of tetrahedrally bonded Si–C bilayers, which are arranged in such a way that different crystal structures from cubic to rhombohedral to hexagonal are formed. This is the reason for the quasi-continuous range of indirect bandgaps from around 2.4 eV to 3.3 eV at 4.2 K [1–5]. Despite the large number of different polytypes, only a few have been thoroughly studied and found their applications in electronic devices in recent years, most notably the 4 H-SiC [6–8].

This phenomenon can be attributed to the wider band gap of 4 H-SiC, which generally provides superior properties for high-power electronics and high-temperature applications. The disparity in interest is evidenced by the fact that there are more than three times as many published studies on 4 H-SiC compared to 3C-SiC. In recent years, nearly exhaustive defect characterization of n-doped 4 H-SiC has been achieved. The primary defects originate from crystal growth, particularly carbon vacancies (V_C), as well as from irradiation and implantation processes involving varying energy levels, which include carbon interstitial atoms (C_i) and silicon vacancies (V_{Si}). In p-doped 4 H-SiC, the B centre (related to boron) and the D

* Author to whom any correspondence should be addressed.

centre (associated with C_i) have been predominantly reported [8, 9].

Another polytype, cubic SiC (also known as β-SiC or 3C-SiC) crystallizes in a simple zincblende structure [6, 10–12]. Because of its superior electrical properties for power electronics a growing interest on this polytype over the last decade is noticeable [6, 7]. Applications like high-frequency microelectromechanical sensors [6], impact ionization avalanche transit time diodes [13, 14], buffer layer properties in ultra thin solar cells [15], in the field of photoelectric hydrogen generation, where the stability and the ideal position of the bandgap relative to that of the water redox potential spread [11], and many others has been reported. Moreover devices build using this polytype can be used in adverse environments such as high temperatures or high particle bombardment which is of interest for many sensor applications in the aerospace industry. Efforts have been made in this area to create SiC based circuits and sensors with high electrical power without additional protection from environmental influences [7, 16, 17]. Another challenge is the relatively high power consumption [7, 18]. Among others, this can be enforced by crystal defects, which can cause a high leakage current in MOS structures with 3C-SiC, for example [10]. Defects in 3C-SiC are also being investigated as potential qubits for quantum applications [19]. Therefore further investigation of the material for better understanding of its properties and possible applications is necessary.

The substrate on which the semiconductor is grown also has an influence on the defects. The different lattice constants of silicon ($a_{\mathrm{Si}} = 5.43$ Å) and 3C-SiC ($a_{3\mathrm{C-SiC}} = 4.36$ Å) and the difference in thermal expansion can lead to the formation of dislocations, stacking faults or voids. The defects can spread out several μm shown in STEM images [6, 20, 21].

Recent calculations using density functional theory supercells in combination with the local moment counter charge method have, been able to determine a defect gap for intrinsic defects that is in good agreement with the experimental band gap of 3C-SiC [22]. Previous studies were limited to smaller supercells and did not converge to reasonable energies. The LMCC method was able to circumvent the Kohn–Sham bandgap problem. For other materials such as Si, CsI, GaAs, this led to a good prediction of the experimental data with an accuracy of 0.1 eV to 0.2 eV [22–25]. However, so far Schultz *et al* lacked the experimental data for a final proof of the calculated defect levels [22].

In the past, only a few deep level transient spectroscopy (DLTS) studies have been carried out on 3C-SiC, as previous investigations have focused more on 4 H-SiC [26–29]. Previous DLTS studies on 3C-SiC investigate defects caused by specific impurities [8, 26, 27], the influence of irradiation, and particle bombardment [8, 28, 30]. However, although some defects, such as carbon vacancies and divacancies with similar properties, have been detected in both 4 H-SiC and 3C-SiC in the past, there are differences due to the polytype-specific structure. [19, 31–33] These have an influence on the formation, migration, and stability of the defect. [8, 19, 31–33] Given the structural differences and the low level of interest in 3C-SiC, a recent review on defects in different SiC polytypes has declared that the characterization of electrically active defects in 3C-SiC is not yet complete [8].

In this study, we investigate electrically active defects in 3C-SiC epitaxial layers grown on Si substrate by DLTS. Capacitive DLTS, commonly referred to as C-DLTS, was developed by Lang *et al* in 1974 [34] and has since become a standard method for characterizing electrical defects in semiconductor devices. This technique was employed in this study due to its relative simplicity and high sensitivity to electrical defects. The results obtained from C-DLTS also serve as a solid foundation that can be easily complemented by more specialized DLTS techniques, such as constant capacitance DLTS (CC-DLTS, sometimes called U-DLTS), which enables a more precise evaluation of the impurity profile, or current DLTS (I-DLTS), which is particularly advantageous for small capacitances or devices with high resistances. However, compared to the other methods, C-DLTS benefits from a more extensive body of comparative literature, facilitating the initial identification of defects.

2. Experimental details

Epi Stacks of differently doped 3C-SiC were grown on a highly-doped *n*-type Si substrate. A schematic structures of the epilayer stacks are shown in figure 1. Depending on the 3C-SiC-epilayer doping and the stack, different ohmic and Schottky contacts were deposited. The *n*-layers were epitaxially grown at 1320 °C. In case of *n*-layer the thickness was 9.1 μm. Figure 1 shows that the ohmic contact was deposited on the front surface. For the samples 100 nm Ni was first deposited by an electron beam evaporation process at 91 °C at 10^{-6} mbar using a shadow mask and then annealed for ohmic contact in a RTP for 300 s at maximal temperature of 1050 °C under Ar atmosphere. Masked 100 nm Ni was deposited as Schottky contact.

Schottky contacts of different sizes were formed on each sample by shadow mask. The electrical measurements were performed using a current voltage (*IV*), capacitance voltage (*CV*) measurements and DLTS setup including a MFIA Impedance Analyser. The setup has been already described elsewhere [35]. *IV*- and *CV*-curves were recorded at 300 K for preliminary characterization. DLTS measurements were performed in the 80–380 K temperature range with 2 K steps. For the each step 200 transients were recorded and averaged to maximize the signal to noise ratio. The reverse bias U_R and the pulse ΔU_p voltage for each sample is shown in table 1. For all samples pulse duration $t_p = 1$ ms and $t_w = 265$ ms transient window were chosen. The reaction time of the MFIA required only 75 μs of delay time, which is fast compared to conventional capacitance transient measurements.

Various rate windows were used to generate different DLTS spectra from the transients measured at various temperatures. For this purpose, the HiRes-4 [36] (also known as GS4 or CS4) and the sine correlation functions were used. Due to the higher

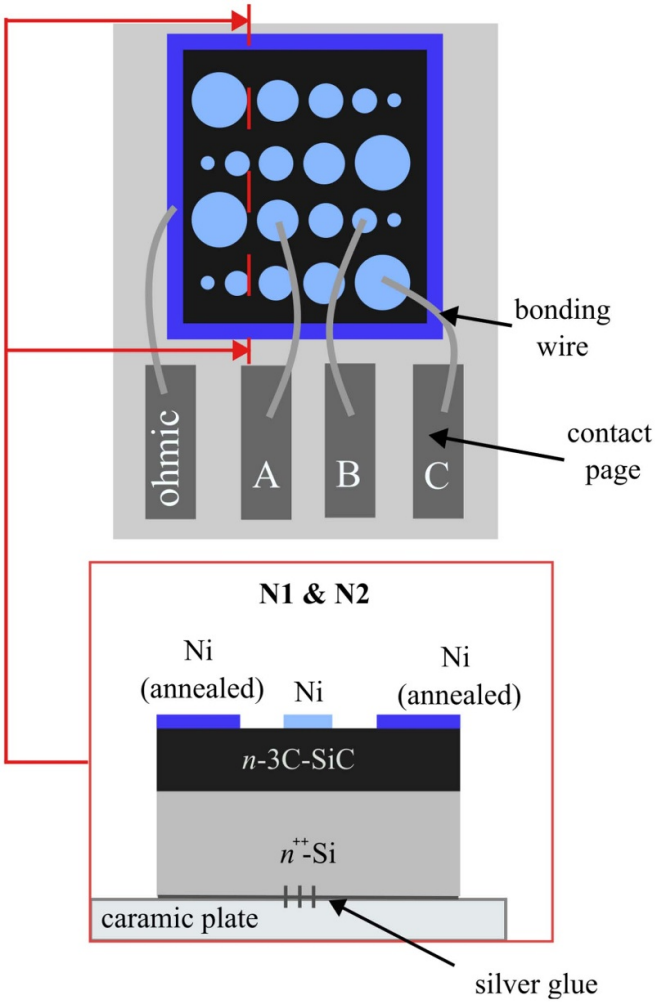

Figure 1. The sketches of the sample structure. Annealed contacts are ohmic, the others behave as Schottky contacts.

resolution, the HiRes-4 correlation procedure were used to determine the number of peaks present. The sine correlation procedure were selected for further analysis due to its higher signal-to-noise ratio and the shape of the peaks, which enables fitting by Gaussian function [36]. Because of the overlapping peaks the fitted peak maxima for every rate window and peak were used to calculate defect concentration N_T by equation (1) where N_D is the dopant concentration and $(\Delta C/C_0)_{max}$ is the peak maxima after the correlation process. ΔC is the amplitude of the averaged transient and C_0 is the stationary capacitance under reverse bias at the end of the transient.

$$N_T \approx 2 \cdot N_D \cdot \left(\frac{\Delta C}{C_0}\right)_{max}. \quad (1)$$

The activation energy $(E_C - E_t)$ and thermal capture cross-section approximation σ were obtained from the Arrhenius plot calculated from the fitted peak maxima.

We would like to point out that, due to the overlap of the peaks, the peak position can be determined accurately, but the peak height is prone to error due to the fitting process.

Table 1. Detailed information of investigated samples as well as applied DLTS measurement parameters. N1 and N2 are the sample type label from figure 1 but from different samples. The letter indicates the measured contact from this sample while the last number separates the measurements on the same sample contact. A is contact area, U_R is reverse bias and ΔU_p is the deviation under plus voltage.

Sample	3C-SiC	A in mm^2	U_R in V	ΔU_p in V
N1-C (1)	*n*-type	1.1387	−6.00	5.00
N1-C (2)	*n*-type	1.1387	−8.00	2.00
N2-C	*n*-type	0.1971	−6.00	5.50

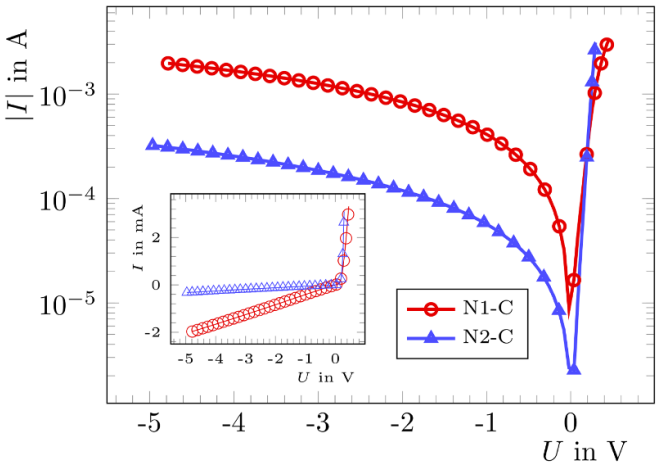

Figure 2. The semi-logarithmic representation of *IV*-curves with dominant behaviour of the *n*-3C-SiC in the material stack. The N1 and N2 *n*-type curves are obtained from two different samples. A linear presentation of all curves is shown in the inset.

Furthermore, there may be additional defects under the broad peaks, but these were not taken into account because (a) they were not visible in all rate windows and (b) to avoid overfitting the spectrum. Consequently, the specified defect concentration can only serve as a rough estimate, whereas the energy level remains accurate within the scope of the measurements. Laplace DLTS measurements could offer an advantage for better separation of the defects.

3. Results and discussion

As seen from the *IV* curves (current I, voltage V, figure 2) and *CV* curves (figure 3), the shapes of the curves depend on doping of 3C-SiC layers. In figure 2, a clear *n*-type behaviour can be observed for samples N1 and N2, which is accompanied by a clear depletion, a low leakage current at negative bias voltage and also a strong increase in current flow at positive bias voltage, as expected for the Schottky diode.

By plotting the $C - V$ measurements in a $(1/C^2)$-plot (see figure 3), the dopant concentrations N_D for the different contacts with depletion could be calculated based on the slope found by linear regression. For the contact N1-C (sample N1, contact C) a voltage range of U_R between –6 V and –1 V was

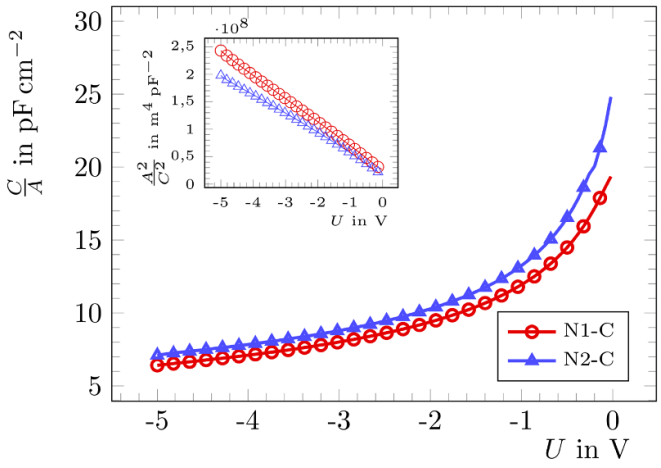

Figure 3. *CV* characteristics of the different *n*-3C-SiC samples. The capacitances are normalized by the contact area. Examples for determination of the net doping concentration are shown in inset of the figure for N1 and N2.

Table 2. The trap concentration was calculated from the fitted intensity at the rate window 1000 Hz using sin correlation procedure. This rate window was chosen because it reaches a maximum for all peaks of the different rate window spectra. Furthermore, the donor concentrations determined by the capacitance measurements at 300 K are also listed.

Sample	N1-C (1)	N1-C (2)	N2-C
N_D in 10^{15} cm^{-3}	3.79	3.79	2.07
T_{peak}		N_T **in 1·10^{11} cm^{-3}**	
105 K (E1)	5.87	2.31	2.72
150 K (E2)	4.13	1.43	3.25
185 K (E3)	1.60	0.34	1.56
220 K (E4)	4.96	2.37	1.61
260 K (E5)	0.66	0.30	1.07
330 K (E6)	21.90	6.79	6.09

used, for the contact N2-C (sample N2, contact C) from U_R −6 V to −0.5 V.

As shown in table 2, N1 and N2 had different contact areas ($1.137{\cdot}10^{-2}$ cm^2 and $1.9713{\cdot}10^{-3}$ cm^2) for DLTS measurements of *n*-3C-SiC. The reverse bias voltage U_R and pulse ΔU_p were varied (see table 1). Figure 4 shows DLTS signals for a 10 Hz rate window, revealing six peaks at similar temperatures across samples.

Differences in N_T between N1-C (1) and N2-C are observed, which are similar for E2 and E3 but show significant differences for E4 and E6 at 220 K and 330 K (table 2). Trap concentrations were calculated from fitted Gaussian peak heights, with most defects estimated at 10^{11} cm^{-3} using the method in section 2. For N1-C (1) and N1-C (2), the defect at 260 K showed a concentration of 10^{10} cm^{-3}. Another outlier is the 330 K peak of N1-C (1), with a concentration of $2.19{\cdot}10^{12}$ cm^{-3}, much higher than that of other samples. However, all calculations should be treated cautiously due to potential errors from overlapping and the fitting process.

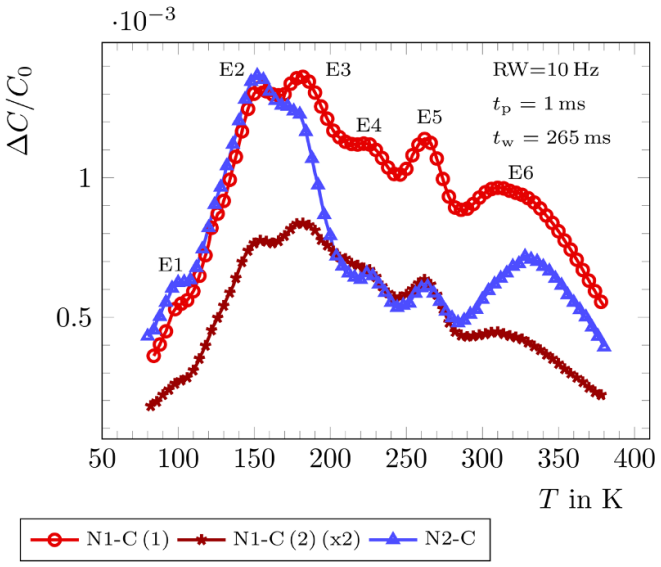

Figure 4. DLTS spectra from *n*-3C-SiC for the different contacts at 10 Hz rate window and sin correlation. The reversed bias and the voltage pulses are varied for the different samples. N1-C1 (1) $U_R = -6$ V, $\Delta U_p = 5$ V, N1-C1 (2) $U_R = -8$ V, $\Delta U_p = 2$ V and N2-C $U_R = -6$ V, $\Delta U_p = 5.5$ V.

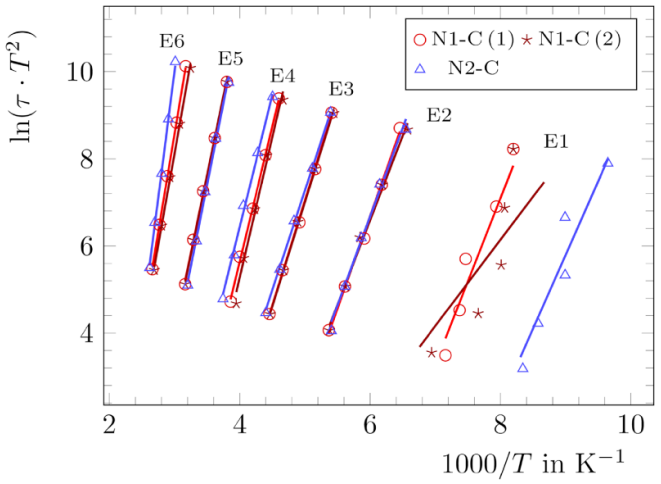

Figure 5. The Arrhenius plot shows the detected dependencies for majority traps for all *n*-type samples. Defect 10^{-1} exhibit a wide spread in the parameters.

Still, a concentration magnitude of 10^{11} cm^{-3} is a reasonable assumption for all defects.

In what follows, the detected electron defects in figure 4 are discussed in more detail. It should be noted that only the observed peaks around 105 K (E1) differ significantly in its fitted peak position between the samples, as shown in the Arrhenius plot in figure 5 and table 3. The 105 K peak may be attributed to two intrinsic defects based on theoretical studies from Schultz *et al* [22]. They defined a defect gap of E_{dg} =2.4 eV, consistent with the experimental bandgap of E_g =2.417 eV at 4.2 K [22, 38]. In this work, the defect energy

Table 3. DLTS *n*-majority trap signals with determined activation energies and apparent capture cross sections. Literature references are listed for the respective peaks. The theoretically predicted activation energies are calculated by Schultz *et al* as explained in the discussion. These values are to be considered with an error of ±0.1 eV. (VV' = V_{Si}–V_C, VV* = V_{Si}–C_{Si}–V_C).

	105 K (E1)		150 K (E2)		185 K (E3)	
T_{peak}(10 Hz)	$(E_C - E_t)$ in eV	σ in cm^2	$(E_C - E_t)$ in eV	σ in cm^2	$(E_C - E_t)$ in eV	σ in cm^2
N1 C (1)	0.329	$6.43{\cdot}10^{-12}$	0.367	$6.39{\cdot}10^{-14}$	0.415	$1.05{\cdot}10^{-14}$
N1 C (2)	0.171	$6.78{\cdot}10^{-18}$	0.334	$7.24{\cdot}10^{-15}$	0.412	$9.42{\cdot}10^{-15}$
N2 C	0.292	$2.19{\cdot}10^{-11}$	0.350	$2.08{\cdot}10^{-14}$	0.393	$2.37{\cdot}10^{-15}$
Reference						
Kato *et al* [28]	—	—	0.33	$3.4{\cdot}10^{-14}$	—	—
Ichimura *et al* [37]	—	—	0.34	$2.2{\cdot}10^{-17}$	—	—
Schultz *et al* [22]	0.17	C_i (−1/0)	0.32	VV'/VV* (0)	0.42	VV* (0)
	0.29	VV'(−1/0)	—	—	—	—

	220 K (E4)		**260 K (E5)**		**330 K (E6)**	
T_{peak}(10 Hz)	$(E_C - E_t)$ **in eV**	σ **in cm^2**	$(E_C - E_t)$ **in eV**	σ **in cm^2**	$(E_C - E_t)$ **in eV**	σ **in cm^2**
N1 C (1)	0.532	$7.69{\cdot}10^{-14}$	0.620	$1.72{\cdot}10^{-14}$	0.773	$3.84{\cdot}10^{-14}$
N1 C (2)	0.551	$2.74{\cdot}10^{-13}$	0.628	$2.43{\cdot}10^{-14}$	0.725	$1.15{\cdot}10^{-14}$
N2 C	0.518	$1.86{\cdot}10^{-14}$	0.647	$6.57{\cdot}10^{-14}$	1.003	$2.80{\cdot}10^{-11}$
Reference						
Kato *et al* [28]	0.50	$2.2{\cdot}10^{-13}$	0.61	1.0×10^{-13}	—	—
Ichimura *et al* [37]	0.52	$5.6{\cdot}10^{-18}$	—	—	—	—
Beyer *et al* [26]	—	—	0.57	$6.0{\cdot}10^{-15}$	—	—
Schultz *et al* [22]	0.57	C_i (0/+1)	0.61	V_c (0/1+)	0.72	Si_i (+1/+2)
	—	—	0.62	Si_i (0/+1)	0.87	Si_i (+2/+3)
	—	—	—	—	1.07	Si_i (+3/+4)

E_t was calculated as $E_a^{theo} = E_{dg} - E_t$, analogous to Arrhenius plot analysis.

For samples N1-C (2) the theoretical and experimental activation energy ($E_a^{theo} = 0.17(\pm 0.1)$ eV) corresponds to a negatively charged carbon interstitial (C_i(−1/0), see table 3). In sample N2-C, the energy ($E_a = 0.292$ eV) matches a negatively charged divacancy (VV'(−1/0), $E_a^{theo} = 0.29(\pm 0.1)$ eV). For E1 in sample N1-C (1), no meaningful energy values could be determined due to evaluation limitations.

The energy of the subsequent peak E2 at 150 K (see figures 4) is slightly shifted to higher activation energies compared to other samples. The activation energies align well with experimental values reported by Kato *et al* [28] ($E_a = 0.33$ eV) and Ichimura *et al* [37] ($E_a = 0.34$ eV), both analysing 3C-SiC on Si. However, neither group provides further details on the origin of these defects. Schultz *et al* [22] report a theoretical value of 0.32 eV for a neutral combined simple divacancy VV' with a side-shifted divacancy VV*, corresponding to the V_{Si}–C_{Si}–V_C complex (VV'/VV*(0)).

The activation energy of E3 at 185 K ranges from 0.393 eV to 0.415 eV, aligning with the theoretical prediction of 0.42(±0.1) eV for a side-shifted divacancy [22]. Defects at 220 K show activation energies from 0.50 eV [28] to 0.52 eV [37], overlapping with our results (0.486 eV to 0.551 eV). These are likely intrinsic defects caused by positively charged carbon interstitials (C_i(0/+1)) with $E_a^{theo} = 0.57(\pm 0.1)$ eV [22]. The E5 DLTS peak, observed between 0.57 eV [26] and 0.61 eV [28], is attributed to carbon vacancies. Further studies suggest this defect is intrinsic, appearing in 3C-SiC on various substrates [39]. Theoretical activation energy of 0.61 (±0.1) eV for V_C(0/+1) matches these findings, though silicon interstitials (0.62 eV) may also contribute, explaining the higher intensity at 220 K.

For the DLTS peak at 300 K (see figure 4), the activation energy varies between 0.725 eV and 1.003 eV. This broad peak, previously observed in 3C-SiC on silicon [30, 39], likely results from overlapping transients of differently charged silicon interstitials (see table 3) [22]. Higher resolution using Laplace DLTS could provide more details, requiring trap concentrations of 10^{-4} to 10^{-2} of the dopant concentration [40]. Samples with higher Si/C ratios may improve this analysis.

As discussed earlier, lattice mismatch between 3C-SiC and Si can cause dislocations and voids. Threading dislocations generated by lattice mismatch between epilayer and substrates are discussed to be the origin of the broadening of DLTS peaks, as in SiGe [41] and GaAs [42, 43]. Point defect agglomerations around dislocations caused by mechanical stresses can also lead to a broadening of the DLTS peaks [44]. Broad and not well-separated peaks in DLTS spectra can also originate from band-like states related to extended defects like dislocations, voids [43] or stacking faults. Further, the dislocation could cause lattice miss-match defects as is know for 3C-SiC. According to recent studies, stacking faults are the main defects in 3C-SiC [21]. To distinguish signals from extended defects from those of point like, dependence on the filling pulse duration should be measured. The dependence of the

DLTS peak maxima and shape on the filling pulse can confirm or exclude the assumption of localized defects near the dislocations, as explained in detail by Gelczuk *et al* [43], and will be a subject of further work.

4. Conclusions

Samples with differently doped layer-stacks of 3C-SiC on high *n*-doped Si were studied. The DLTS investigations showed presence of several defect signatures already known for the SiC films grown on Si. These defects could be detected in the Schottky contact of the *n*-doped 3C-SiC. However, to the best of our knowledge, for the signals reported in previous studies, origin was not discussed so far except the peak at 260 K, which has already been assumed to be an intrinsic defect [39]. Nevertheless, for the defects E2 (150 K), E4 (220 K) and E5 (260 K) the activation energies and the thermal capture cross-sections could be confirmed by experimental results from other studies [26–28, 37, 39].

By comparing new theoretical calculations of intrinsic defects in 3C-SiC by Schultz *et al* [22], all DLTS signals were attributed to intrinsic defects with concentrations around 10^{11} cm^{-3}. The defects likely involve vacancies and interstitials near or as a result from threading extended defects. This is supported by the broader and overlapping peaks. Dislocations and stacking faults from the 3C-SiC/Si lattice mismatch, as reported in STEM studies, may influence defect formation [6, 21]. In particular, stacking defects are considered in the literature to be the main defects in SiC/Si structures [21]. Further studies, such as varying the filling pulse duration t_p, are needed for clarification.

For E5 at 260 K we assumed a superposition of a carbon vacancy V_C with a silicon interstitial Si_i. Furthermore, different charge states of the silicon interstitial could be the reason for peak E6 (330 K). A better energetic resolution, e.g. with Laplace-DLTS, could provide further information here. However, Laplace-DLTS may be very challenging due to the low trap concentration relative to the dopant concentration, which is lower than the usually required 10^{-4} to 10^{-2}.

Data availability statement

All data that support the findings of this study are included within the article (and any supplementary files).

Acknowledgments

We would also like to thank S Seidel, F Weichelt and A Schmid for their contribution to the sample preparation. This work was supported by the Fraunhofer Internal Programs under Grant No. Attract 079-600865, by Enterprise Ireland Commercialisation Fund Project CF20180960 (Schottky-Barrier Diodes on 3C-SiC/Si substrates - 3CSBD) and co-funded by the European Regional Development Fund (ERDF) under Ireland's European Structural and Investment Funds (ESIF) Programme 2014–2020.

Author contributions

P U Feiler 0009-0005-4131-7324
Conceptualization (lead), Data curation (lead), Investigation (lead), Visualization (lead), Writing – original draft (lead), Writing – review & editing (lead)

T Mchedlidze 0000-0003-4514-2734
Data curation (supporting), Supervision (equal), Writing – review & editing (supporting)

K Cherkaoui 0000-0002-7062-5570
Project administration (equal), Resources (lead), Writing – review & editing (equal)

P Ward
Resources (equal), Writing – review & editing (supporting)

A Blake 0000-0001-7961-4459
Funding acquisition (lead), Project administration (lead), Resources (equal), Writing – review & editing (supporting)

J Heitmann 0009-0000-8498-3603
Resources (equal), Supervision (equal), Writing – review & editing (supporting)

F C Beyer 0000-0002-1727-7511
Conceptualization (supporting), Funding acquisition (lead), Project administration (lead), Supervision (equal), Writing – original draft (supporting), Writing – review & editing (supporting)

References

[1] Choyke W J and Pensl G 1991 Siliciumkarbid — Halbleiter für die neunziger Jahre *Phys. Blätter* **47** 212–4
[2] Via F L Severino A, Anzalone R, Bongiorno C, Litrico G, Mauceri M, Schoeler M, Schuh P and Wellmann P 2018 From thin film to bulk 3C-SiC growth: understanding the mechanism of defects reduction *Mater. Sci. Semicond. Process.* **78** 57–68
[3] Matsunami H 1993 Growth and application of cubic SiC *Diam. Relat. Mater.* **2** 1043–50
[4] Wesch W 1996 Silicon carbide: synthesis and processing *Nucl. Instrum. Methods Phys. Res. B* **116** 305–21
[5] Fissel A *et al* 2003 Artificially layered heteropolytypic structures based on SiC polytypes: molecular beam epitaxy, characterization and properties *Phys. Rep.* **379** 149–255
[6] Acharyya A, Biswas A and Das P 2022 *Generation, Detection and Processing of Terahertz Signals* 1st edn (Springer) (https://doi.org/10.1007/978-981-16-4947-9)
[7] Via F L Alquier D, Giannazzo F, Kimoto T, Neudeck P, Ou H, Roncaglia A, Saddow S E and Tudisco S 2023 Emerging SiC applications beyond power electronic devices *Micromachines* **14** 1200
[8] Capan I 2025 Electrically active defects in 3C, 4H and 6H silicon carbide polytypes: a review *Crystals* **15** 0255
[9] Etzelmüller Bathen M , Karsthof R, Galeckas A, Kumar P, Kuznetsov A Y, Grossner U and Vines L 2024 Impact of carbon injection in 4H-SiC on defect formation and minority carrier lifetime *Mater. Sci. Semicond. Process.* **176** 108316
[10] Li F *et al* 2021 Status and prospects of cubic silicon carbide power electronics device technology *Materials* **14** 5831

[11] Jian J and Sun J 2020 A review of recent progress on silicon carbide for photoelectrochemical water splitting *Solar RRL* **4** 2000111
[12] Levinštejn M E, Rumyantsev S L and Shur M (eds) 2001 *Properties of Advanced Semiconductor Materials GaN, AlN, InN, BN, SiC, Sige* (Wiley) p 0471358274
[13] Acharyya A *et al* 2022 Search of a suitable heterojunction material system for terahertz wave generation *Generation, Detection and Processing of Terahertz Signals* vol 794 (Springer) pp 223–38
[14] Ghosh M and Biswas A 2021 Material systems for realizing heterojunction IMPATT sources for generating terahertz waves *Advanced Materials for Future Terahertz Devices, Circuits and Systems* (Springer) pp 261–75
[15] Ali Z , Ali K, Hussain B, Maqsood S and Iqbal I 2022 Towards the enhanced efficiency of ultrathin Sb_2Se_3 based solar cell with cubic silicon carbide (3C–SiC) buffer layer *Opt. Mater.* **128** 112358
[16] Peng G , Zhou Y, He Y, Yu X, Zhang X A, Li G Y and Haick H 2015 UV-induced SiC nanowire sensors *J. Phys. D: Appl. Phys.* **48** 055102
[17] Chen J , Zhang J, Wang M and Li Y 2014 High-temperature hydrogen sensor based on platinum nanoparticle-decorated SiC nanowire device *Sens. Actuators B* **201** 402–6
[18] Zekentes K , Choi J, Stambouli V, Bano E, Karker O and Rogdakis K 2022 Progress in SiC nanowire field-effect-transistors for integrated circuits and sensing applications *Microelectron. Eng.* **255** 111704
[19] Gordon L, Janotti A and van de Walle C G 2015 Defects as qubits in 3C- and 4H-SiC *Phys. Rev. B* **92** 045208
[20] Jinschek J 2001 Different void shapes in Si at the SiC thin film/Si(111) substrate interface *J. Electron Microsc.* **50** 3–8
[21] Litrico G *et al* 2018 Stacking faults defects on 3C-SiC homo-epitaxial films *Mater. Sci. Forum* **924** 124–7
[22] Schultz P A, van Ginhoven R M and Edwards A H 2021 Theoretical study of intrinsic defects in cubic silicon carbide 3C-SiC *Phys. Rev. B* **103** 195202
[23] Schultz P A *et al* 2015 The E1-E2 center in gallium arsenide is the divacancy *J. Phys. Condens. Matter* **27** 075801
[24] van Ginhoven R M and Schultz P A 2013 Off-center Tl and Na dopant centers in CsI *J. Phys. Condens. Matter* **25** 495504
[25] Schultz P A and von Lilienfeld O A 2009 Simple intrinsic defects in gallium arsenide *Modelling Simul. Mater. Sci. Eng.* **17** 084007
[26] Beyer F C Hemmingsson C G, Gällström A, Leone S, Pedersen H, Henry A and Janzén E 2011 Deep levels in tungsten doped n-type 3C–SiC *Appl. Phys. Lett.* **98** 152104
[27] Beyer F C *et al* 2010 Deep levels in hetero-epitaxial as-grown 3C-SiC *AIP Conf. Proc.* **1292** 63–66
[28] Kato M, Sobue F, Ichimura M, Arai E, Yamada N, Tokuda Y and Okumura T 2001 Passivation of deep levels in 3C-SiC on Si by a hydrogen plasma treatment *Jpn. J. Appl. Phys.* **40** 2983
[29] Bathen M E , Coutinho J, Ayedh H M, Ul Hassan J, Farkas I, Öberg S, Frodason Y K, Svensson B G and Vines L 2019 Anisotropic and plane-selective migration of the carbon vacancy in SiC: theory and experiment *Phys. Rev. B* **100** 014103
[30] Kato M , Ichimura M, Arai E and Tokuda Y 2003 Deep level characterization and its passivation in 3C-SiC monitored by capacitance transient methods *Defect Diffus. Forum* **218–220** 1–16
[31] Alfieri G and Kimoto T 2009 Capacitance spectroscopy study of midgap levels in n-type SiC polytypes *Silicon Carbide and Related Materials 2008* vol 615 (Trans Tech Publications Ltd) pp 389–92
[32] Posselt M, Gao F, Weber W J and Belko V 2004 A comparative study of the structure and energetics of elementary defects in 3C- and 4H-SiC *J. Phys.: Condens. Matter* **16** 1307
[33] Liao T, Roma G and Wang J 2009 First-principles study of neutral silicon interstitials in 3C- and 4H-SiC *Phil. Mag.* **89** 2271–84
[34] Lang D V 1974 Deep-level transient spectroscopy: a new method to characterize traps in semiconductors *J. Appl. Phys.* **45** 3023–32
[35] Mchedlidze T 2023 Pros for using MFIA in deep level transient spectroscopy studies (https://doi.org/10.13140/RG.2.2.19774.25920)
[36] Istratov A A, Vyvenko O F, Hieslmair H and Weber E R 1998 Critical analysis of weighting functions for the deep level transient spectroscopy of semiconductors *Meas. Sci. Technol.* **9** 477–84
[37] Ichimura M , Koga Y, Yamada N, Abe T, Arai E and Tokuda Y 1998 Study of carrier emission and capture processes at electron traps in 3C-SiC *Jpn. J. Appl. Phys.* **37** L18
[38] Humphreys R G, Bimberg D and Choyke W J 1981 Wavelength modulated absorption in SiC *Solid State Commun.* **39** 163–7
[39] Henry A , Leone S, Beyer F C, Andersson S, Kordina O and Janzén E 2011 Chloride based CVD of 3C-SiC on (0001) α-SiC substrates *Mater. Sci. Forum* **679–680** 75–78
[40] Schroder D K 2006 Defect *Semiconductor Material and Device Characterization* (Wiley) pp 251–317
[41] Ringel S A and Grillot P N 1996 Dislocation interactions and their impact on electrical properties of GeSi-based heterostructures *MRS Online Proc. Libr.* **442** 313–24
[42] Yastrubchak O , Wosiński T, Mąkosa A, Figielski T and Tóth A L 2001 Capture kinetics at deep-level defects in lattice-mismatched GaAs-based heterostructures *Physica B* **308–310** 757–60
[43] Gelczuk L, Dabrowska-Szata M and Józwiak G 2005 Distinguishing and identifying point and extended defects in DLTS measurements *Mater. Sci.* **23** 0137–1339
[44] Kisielowski C and Weber E R 1991 Inhomogeneities in plastically deformed silicon single crystals II: deep-level transient spectroscopy investigations of *p*- and *n*-doped silicon *Phys. Rev. B* **44** 1600–12